Thermodynamic equilibrium approach to predict the inorganic interactions of ash from biomass and their mixtures: A critical assessment

Emile Atallah, Françoise Defoort, Alexander Pisch, Capucine Dupont

Thermodynamic equilibrium approach to predict the inorganic interactions of ash from biomass and their mixtures: a critical assessment[1]

Emile ATALLAH[1], Françoise DEFOORT[1], Alexander PISCH[2], Capucine DUPONT[3]

[1] Université Grenoble Alpes, Commissariat à l'Energie Atomique et aux Energies Alternatives (CEA), Laboratoire d'Innovation pour les Technologies des Energies nouvelles et les Nanomatériaux (LITEN), DTCH, F-38000 Grenoble, France
[2] Université Grenoble Alpes, CNRS, Grenoble INP, SIMaP, 38000 Grenoble, France
[3] IHE Delft Institute for Water Education, Department of Water Supply Sanitation and Environmental Engineering, Delft, the Netherlands

Abstract

Process simulation approaches based on thermodynamics calculations can provide good capabilities to predict the ash behavior of biomasses and their mixtures. In the present work, a critical assessment of such simulations was performed in the field of biomass ashes, and experimentally checked to be at equilibrium. Two commercial thermodynamic databases, FToxid and GTOX, were used together with the FactSage Gibbs energy minimization software. For the first time in literature, a comparison was performed between the calculated phase equilibria using the recent market versions of the two databases. The predicted results were then compared to those measured on various ash samples of straws and barks along with their ash mixtures, highlighting the lingering need for improvements for the recent versions of these commercial databases.

The phase diagram approach showed excellent capabilities in predicting the physical state of the ash (solid, liquid, or solid-liquid mixture) using both databases. Global simulations using the FToxid database showed better prediction capabilities for single biomass ash than those using the GTOX database. Unfortunately, predictions using the former were significantly limited in the case of ash mixture samples, whereas using the latter were a total failure. Nevertheless, both databases showed correct volatilization prediction capabilities but failed to forecast the solidus and liquidus characteristic temperatures. Further work is still needed to enhance the prediction capabilities of this tool.

Keywords: Biomass ash, biomass ash mixtures, thermodynamic equilibrium, global thermodynamic simulation, ash behavior prediction, phase diagram CaO-K_2O-SiO_2.

[1] Paper published in : *Fuel Processing Technology*, *235* (2022) 107369.

1. Introduction

A decade ago, Morey et al. [1] were the first to investigate the phase relations in the ternary $CaO\text{-}K_2O\text{-}SiO_2$ system. Compositions in this ternary are used in the glass production industry, such as bottles, containers, etc. [2]. This system is also relevant for advanced ceramic applications, such as in biocompatible ceramic material production for biomedical applications [3]. Most importantly, around 90 wt.% of biomass ash is formed of silicon, potassium, and calcium [4]. Hence, a thorough knowledge of the phase equilibria in the $CaO\text{-}K_2O\text{-}SiO_2$ ternary system can help better understand and predict the complicated chemical interaction of the inorganic elements in the biomass ash in real-life processes during combustion and gasification.

High alkali-silicate biomasses, such as agricultural residues, often result in ashes with low melting points [5]. This can cause corrosion and sintering in a furnace or lead to a reaction with the bed materials in the fluidized bed and cause agglomeration [6–8]. Therefore, mixing agricultural residues with biomasses with high melting points, such as oak bark, can alter the chemical and physical properties of the ashes in the mixture, hindering the ash-related problematics [5,9–11].

Advanced multicomponent/multiphase thermodynamic modeling can be an important tool in predicting ash-related processes in biomass combustion. Thermodynamic modeling can predict the ash deposition, corrosion, bed agglomeration of fluidized beds, and ash interaction and compositions. However, consistent and accurate thermodynamic data are needed for all the ash phases that may form in furnace and boiler conditions [12]. This prediction tool can be more efficient than the costly and time-consuming random mixing approach. In addition, it helps to control the operational problems related to ash, hence inducing economic savings. The FactSage software package and its thermodynamic databases are widely used to perform phase diagram calculations and process-related simulations based on proper thermodynamic equilibrium constraints. The thermodynamic databases FToxid [13] and GTOX [14] in their most recent versions are most relevant for use in simulations of ash formation during biomass combustion. In general, authors in the literature tend to use the FACT database package without a detailed explanation for their choice.

Recent literature works investigated the capabilities of such an approach to predict the combustion ash behavior of biomasses and their blends. For instance, Wiinikka et al. [15] investigated the influence of fuel ash composition on high-temperature aerosols formation during fixed-bed combustion of woody biomass (two wood pellets and one bark pellet) in a

laboratory reactor compared to theoretically chemical equilibrium model calculations (FactSage 5.2 with FACT and SGTE databases). In parallel, Elled et al. [16] investigated the composition of agglomerated materials. They aimed to highlight the reasons for sintering and agglomeration during the thermochemical conversion of bark and its blend with straw. They compared their experimental results in a 12 MW circulating fluidized bed reactor (using quartz sand as bed material) against thermodynamic equilibrium modeling using FactSage 6.2 equipped with FTSalt, FToxid, and Fact53 databases.

In addition, Rizvi et al. [17] compared the predicted slagging results by ash fusion tests on soft-wood, peanut shell, sunflower husk, and miscanthus with those simulated by FactSage 6.3 equipped with FToxid and FactPS databases using all the elements and at varying temperatures between 700°C and 1500°C. Reinmoller et al. [18] also used FactSage 6.3 equipped with FToxid, FatcPS, FTSalt, and FTmisc databases in air on 23 different biomasses (including wood, bark, and straw) to investigate the slag and the mineral phase composition compared to experimental data (ash fusion test). More recently, Magdziarz et al. [19] used the same approach on three wood and one straw samples. Dizaji et al. [20] tried to study wheat straw's combustion ash transformation reactions using an experimental ash test (ash annealing) compared with calculated results from simulations done with FactSage 8.0 equipped with FToxid, FTSalt, and FactPS databases at various temperatures. Link et al. [21] also used the same simulation approach (but with FactSage 7.3) compared with the standard ash melting test to assess the melting behavior and ash phase transformation in wood, reed, and their blends. In addition, Fakourian et al. [22] tried to model the ash deposit growth rates and the melting fraction and temperature for a wide range of solid fuels (including woody biomass) in a 100 kW combustor using a simulation approach using FactSage 7.3.

All these authors reported the limited success of this tool in predicting the real ash behavior of biomass and their mixtures compared with the experimental findings. For instance, the predicted amounts of the crystalline compounds were always different from those measured [17–19]. The predicted melting temperatures also differed from those measured [18,19,21], which was the same case for the slagging proportion [20]. Though the aerosol predicted values showed a preliminary match against the measured P-XRD results, some experimental values were not initially at equilibrium due to temperature or residence time limitations, which further biased the prediction [15].

In his recent review, Lindberg et al. [12] summarized the leading cause of all these limitations as the lack of comprehensive databases containing the thermodynamic data of ash compounds

and phases formed during combustion. Elled et al. [16] reported that this same problem led to a biased predicted value for the agglomeration temperature (deviated liquidus temperature compared to experimental results). Elled et al. [16] further elaborated that the thermodynamic equilibrium assumes a complete reaction of the ash, which might not be the real life case [16]. Hence, deviations between the thermodynamic equilibrium behavior and the real one always remained.

On the other hand, the phase relationships in the ternary phase diagram $CaO-K_2O-SiO_2$ consist of a more simplified prediction approach. In general, the authors in the literature normalize the CaO, K_2O, and SiO_2 mole or weight percentages from the measured elemental compositions on each biomass or blend. Then, they position the feedstock on the calculated ternary phase diagram $CaO-K_2O-SiO_2$ to get some qualitative information on its ash behavior. For instance, Ohman et al. [7] used this diagram to qualitatively predict the presence of slag in wheat straw, wood, peat, cane trash, wood residues, reed canary grass, bark, and RDF in a fluidized combustion bed. Similarly, Rebbling et al. [6] used phase equilibria information of this ternary diagram to predict the slag formation of wood, peat, and their mixtures in three separate grate-fired combustion boilers of different sizes, 0.2 MWth, 2MWth, and 4 MWth, respectively. In addition, Defoort et al. [9] used this phase diagram information to predict the ash state (solid, liquid, or solid-liquid) of oak bark, wheat straw, and their mixtures in two different laboratory-scale combustion tests using biomass pellets and ash chips. Zhu et al. [23] also tried to verify the deformation temperatures of more than 15 biomasses (including wood and straw). They compared the experimental results on a laboratory scale against the thermodynamic equilibrium information of this ternary phase diagram (using their normalized oxides percentages) after adding Al_2O_3 as a fourth oxide to the system.

All these authors reported the success of this tool in predicting the state of the total ash after combustion. However, some crystalline phases appeared experimentally but were absent in the thermodynamic database, such as $K_2Ca_6Si_4O_{15}$ and $K_2Ca_2Si_2O_7$ [9]. Others were predicted but were never found experimentally, such as K_2CaSiO_4 [9]. In addition, the calculated liquidus line was shifted compared with the experimental results [6,7,23]. Consequently, they all concluded that the thermodynamic database needs to be revised to calculate the equilibria in the entire composition and temperature space. Recent thermodynamic improvements were made to the FACT database package (especially FToxid) in 2017 [24], but they still need to be assessed against experimental data.

This work aims to assess the capabilities of using the most recent versions of these thermodynamic databases to predict the interactions between the inorganic elements (i.e., phase relationships) in the ash of biomass and their mixtures. First, for the first time in the literature, a comparison was performed between the calculated phase equilibria obtained with the two databases (FToxid vs. GTOX) regarding predicted crystalline phase compositions and volatilization behavior. Two prediction approaches were used as done previously [9,25]: a simplified one using phase diagram calculations and a more sophisticated one called global simulation. Both approaches were then compared to experimental results on multiple ash samples already checked to be at equilibrium (from single biomass and mixtures) [26]. This aimed to evaluate the thermodynamic approach prediction capabilities using the most recent databases and suggest improvements.

2. Materials and methods

2.1. Feedstock

Oak bark, wheat straw, and two mixtures were received in the form of compressed pellets (1.5cm (L) x 0.5cm (D)). Three different barks and three different wheat straw sources were used:

- Two oak barks (BC and BF) sawmill residues from the southwest of France and a hardwood bark (BI) residue from Italian logs preparation in the wood industry.
- Two wheat straws (WC and WF) from the southwest French agriculture industry and a wheat straw (WI) residue from the Italian one.

The BCWC mixture was prepared by Defoort et al. [9], and the BFWF blend was received as a pellet in the work of Valin et al. [27]. The other mixtures were formed manually. Single biomass pellets were ground in a Fisher Bioblock Scientific Retsch grinder below 1 mm. After drying the biomass powder at 105°C for 24h, bark-straw mixtures of 5 g each were put in a plastic bottle and mixed in a "turbula" mixer (Willy A. Bschofen AG Maschinenfabrik CH-4005 Basel/Schweiz mixer), with various bark weight fractions (α) (Table 2). The bark weight fraction (α) of each biomass mixture (Table 2) was varied to cover a considerable part of the CaO-K_2O-SiO_2 phase diagram.

Afterward, each biomass pellet and the ground mixtures were ashed at 550°C for 2h in natural air with the same procedure as detailed in Atallah et al. [26]. This step at 550°C removed all organic oxygen and hydrogen (along with organic nitrogen and part of chlorine) while preserving the majority of the other elements. Then 0.5 g of ash from each mixture and single

biomasses were compressed as ash chips with the same procedure described in Atallah et al. [26] to favor the contact between the inorganic ash particles.

Note that the bark weight fraction in the ash bark-straw mixture (β) can be calculated using the bark weight fraction in the biomass bark-straw mixture (α), taking into account the ash yield of every single biomass (noted A_1 for bark and A_2 for straw) and is:

$$\beta = \alpha A_1/(\alpha A_1 + (1-\alpha)A_2) \quad (1)$$

For instance, a BCWC biomass mixture of 50% biomass bark weight percentage corresponds to an ash mixture of 59% ash bark weight percentage in the mixture.

The elemental composition of each single biomass ash (Table 1) and ash mixture (Table 2) was measured by an Elementar Vario EL cube CHN analyzer along with an inductively coupled plasma atomic emission spectroscopy (ICP−AES) for Si, Ca, K, P, Al, Mg, Fe, Na, and Mn. C (std = ±1%), H (std = ±2%), and N (std = ±15%) contents were measured according to the NF EN 15104 norm. Ca, K, P, Al, Mg, Fe, Na, and Mn amounts were measured according to the NF EN ISO 16967 norm (std = ±5%). The amounts of S and Cl were evaluated in an ion chromatography after combusting the samples in a bomb calorimeter, according to the EN 15289 norm (std = ±15%). Si contents were measured by an internal ICP method (std = ±5%). The weight percentage of the oxides of interest (CaO, K_2O, and SiO_2) in every biomass and mixture was calculated based on Ca, K, and Si contents measured by the ICP-AES. The values are reported in Tables 1 and 2.

Table 1: Biomass ash elemental composition on a dry basis along with their SiO_2, CaO, and K_2O weight percentages.

All elements in wt.% ash	**WC**	**WF**	**WI**	**BC**	**BF**	**BI**
C	4.360	1.200	0.900	4.860	6.100	6.400
O	45.140	44.705	41.933	52.003	51.993	46.233
S	0.940	1.404	1.755	0.378	0.088	0.377
Cl	0.141	0.329	0.113	0.007	0.005	0.008
Si	17.095	25.351	18.520	5.699	10.351	8.693
Ca	5.045	4.036	6.924	30.462	25.271	25.101
K	24.667	20.192	25.066	3.108	2.402	7.837
P	1.160	1.215	1.673	0.380	0.229	0.862
Al	0.076	0.107	0.612	0.874	1.414	1.100
Mg	0.795	1.098	1.364	0.860	0.534	1.887
Fe	0.141	0.127	0.563	0.412	1.034	0.907
Na	0.355	0.165	0.460	0.138	0.237	0.556
Mn	0.084	0.070	0.117	0.820	0.342	0.040

Ash 550°C (wt.%)	5.8	8.47	3.98	8.4	11.68	8.3
SiO2	*49.9%*	*64.4%*	*49.9%*	*20.8%*	*36.7%*	*29.5%*
CaO	*9.6%*	*6.7%*	*12.2%*	*72.8%*	*58.5%*	*55.6%*
K2O	*40.5%*	*28.9%*	*37.9%*	*6.4%*	*4.8%*	*14.9%*

Table 2: Biomass ash mixtures elemental composition on a dry basis along with their SiO_2, CaO, and K_2O weight percentages.

All elements in wt.% ash	**BCWC**	**BCWI**	**BCWF**	**BIWC**	**BIWI**	**BFWC**	**BFWI**	**BFWF**
α	0.500	0.314	0.559	0.616	0.550	0.352	0.242	0.500
β	0.590	0.490	0.557	0.697	0.718	0.522	0.484	0.580
C	6.30	5.20	5.50	5.00	4.60	4.40	4.00	4.90
O	45.75	46.24	48.75	47.95	46.79	48.62	50.34	47.19
S	0.79	0.76	0.64	0.56	0.65	0.80	Not measured	0.56
Cl	0.56	0.36	0.45	0.34	0.26	0.61	Not measured	0.29
Si	11.62	11.10	13.40	14.30	13.40	13.50	14.00	16.00
Ca	20.95	20.49	18.83	13.47	15.90	14.69	15.37	17.37
K	11.00	12.27	9.38	13.15	12.44	14.21	12.34	10.18
P	0.55	0.73	0.46	0.83	1.04	0.66	0.75	0.52
Al	0.82	0.75	0.80	1.59	1.69	0.85	1.05	1.16
Mg	0.71	1.04	0.72	1.44	1.66	0.68	0.95	0.76
Fe	0.45	0.59	0.67	0.78	0.89	0.53	0.73	0.70
Na	0.26	0.22	0.16	0.54	0.61	0.27	0.25	0.16
Mn	0.26	0.25	0.23	0.06	0.07	0.19	0.22	0.21
Ash 550°C (wt.%)	7.10	5.37	8.43	7.34	6.36	7.87	5.84	10.08
SiO2	*36.9%*	*35.4%*	*43.3%*	*46.9%*	*43.5%*	*43.4%*	*45.2%*	*48.4%*
CaO	*43.4%*	*42.6%*	*39.7%*	*28.8%*	*33.7%*	*30.9%*	*32.4%*	*34.3%*
K2O	*19.6%*	*22.0%*	*17.0%*	*24.2%*	*22.7%*	*25.7%*	*22.4%*	*17.3%*

2.2. Experimental procedure

The compressed ash chips were annealed with the same procedure as in the "ash test" of Atallah et al. [26]. A 95-5 wt.% Pt-Au crucible was used in each experiment. This material was selected to avoid any interaction between the sample and the crucible. It was shown by Atallah et al. [26] that equilibrium for the bark-straw BCWC mixture was experimentally reached at 850°C in 24h, 1000°C in 6h, and 1200°C in 6h [26]. Consequently, all the experiments using the other mixtures were conducted at 1000°C and 6h in air. These laboratory conditions favor chemical reactions and should lead to a final phase assemblage close to thermodynamic equilibrium (high proximity of ash grains).

2.3. P-XRD analysis

A Bruker D8 Advance Powder X-Ray diffraction (P-XRD) equipped with Cu Kα (40 kV and 30 mA) radiation was used to analyze the crystallographic composition and the amorphous contents in each sample. Samples were manually ground in an agate mortar, placed in an amorphous silica sample holder, and then flattened with glass to obtain a well-defined surface. Diffractograms were obtained over a 2θ interval between 15° and 70°. The identification and semi-quantification of the crystalline phases were first performed using the Bruker EVA software and its I/Icor module. Afterward, 10 wt.% of TiO_2 Anatase (99.99 wt.%, Sigma-Aldrich) was added as an internal standard to quantify the amorphous phase (assumed to be a solidified liquid silica-rich phase). Then, full XRD quantification was conducted by applying Rietveld refinement to each sample using the Panalytical Instruments Highscore plus software. The ICDD 2020 crystallography database was used in the software mentioned above. The detailed procedure can be found in the work of Atallah et al. [15].

2.4. Total and elemental weight loss analysis

2.4.1. Total weight loss analysis

The total weight loss was measured from the ash test experiments described in section 2.2 using a mass balance (± 0.001 g) between the beginning of each experiment and its end. In parallel, a SETARAM Setsys 16/18 EO simultaneous thermogravimetric analysis-differential thermal analysis (TGA-DTA-MS) was used to evaluate the dynamic weight loss and differential heat flow as a function of temperature. A piece of compressed ash chip (1.3 cm diameter compressed at a pressure of 10 bar) of BCWC mixture was used as the sample. It was put in a 3 mm diameter x 8 mm height Pt crucible (~70 mg) under air flow rate (50 mL/min). The TGA program was composed of a 10K/min ramp until 1350°C followed by a 30 min plateau and a slow cooling (10°C/min), and a 1h plateau and fast cooling (33°C/min). The detailed results and analysis methods are presented in Appendix D.

2.4.2. Elemental weight loss (or elemental volatilization)

The elemental weight loss (L_i) was calculated using the proportionality rule from the ICP-AES results in Table 2 as follows:

$$L_i = \left(1 - \frac{(1-m_t) \times m_{fin,i}}{m_{in,i}}\right) \times 100 \quad (2)$$

Where $m_{in,i}$ denotes the weight of each element (i) measured by the ICP-AES in the BCWC mixture at 550°C (Table 2), and $m_{fin,i}$ denotes the one measured after annealing at 1000°C or 1200°C.

2.5. Phase diagram calculation and global simulation

All thermodynamic equilibrium calculations and simulations were performed assuming that all elements and phases are homogeneously distributed and available for reaction.

2.5.1. Phase diagram approach

Calculations of the ternary phase diagram K_2O-CaO-SiO_2 (Figure 1) were conducted using the "phase diagram" module of FactSage (version 8.1, June 2021) at three different temperatures (850°C, 1000°C, 1200°C) with GTOX (2018) and FToxid 8.1 (2021) databases. GTOX and FToxid are among the widely used thermodynamic databases in the market that contain thermodynamic data for oxides and their solutions. GTOX modeling was based on the work of Hack et al. [14], while FToxid modeling was based on the work of Kim et al. [24,28].

2.5.2. Global simulation approach

Global simulations of predicted amounts of crystalline phases, liquid slag, and volatilization behavior were conducted to assess further the database quality. The main difference between the global simulation and the phase diagram approach is that the latter uses only Ca, Si, and K oxides without gas. At the same time, the former considers the concentration of the other elements and the gaseous atmosphere (air). The FactSage software was also used to conduct the simulations using its "Equilib" module. Two sets of databases were applied for database comparison:

- Set 1: GTOX (version 2018) for oxides (compounds & solutions) combined with FactPS (June 2021) for the gas species and additional inorganic solid phases.
- Set 2: FToxid 8.1 (June 2021) for oxides (compounds & solutions) combined with FactPS (June 2021) for the gas species and additional inorganic solid phases and FTSalt (June 2021) for salt melts and solutions.

The SGTE pure substance database is usually recommended with GTOX [29], but the authors did not have access to it. Hence, it was replaced by FactPS in dataset 1. The thermodynamic data of FTSalt are compatible with FToxid but not with GTOX. Hence, FTSalt was used with the former rather than with the latter.

The comparison of the predicted results using the global simulations between the two sets of databases was conducted using the elemental analysis of only BC and WC ashes in Table 1 since the analyses were similar to the other biomass ashes. Since the global simulation for the database comparison was conducted on ash samples, bark weight fraction in the ash bark-straw mixture (β) was used. In the simulations, the bark weight fraction in the ash samples (β) was

varied between 0 and 1 in air. A simulation temperature of 1000°C was set, at which equilibrium was experimentally reached in previous work using the same raw materials [26].

Afterward, the elemental analysis of each ash sample from single biomasses and mixtures in Tables 1 and 2 was used to simulate the experimental ash test. 0.5 g of compressed ash chips were applied in this laboratory test. Hence, the simulation inputs from Table 2 were converted to per 0.5 g ash. The partial pressure of oxygen was kept constant by setting its activity at 0.21 during the simulation since the experimental reactions were conducted in a 0.7 L vertical laboratory furnace opened to air. The weight of nitrogen inside the reactor was calculated using the ideal gas equation at 1 atm and 1000°C. It was found to be 0.147 g/h. Since the experiments were conducted for 6h, the added nitrogen weight to the feedstock in the inputs of the simulations was 0.882 g.

3. Results and discussion

3.1. Predicted results comparison between the thermodynamic databases

In this section, calculated results using the GTOX and FToxid thermodynamic databases were compared against each other in terms of the phase diagram approach (section 3.1.1.) and the global simulation approach (section 3.1.2.).

3.1.1. Phase diagram approach

The CaO-K_2O-SiO_2 ternary phase diagram may have the capability to predict the state of the biomass ash and their ash mixtures, i.e., if they are in the solid, the liquid, or the solid-liquid phases. In Figure 1, the calculated isothermal sections of the ternary phase diagrams CaO-K_2O-SiO_2 at 850°C, 1000°C, and 1200°C using GTOX and FToxid were shown. The green sections referred to the pure solid region, while those in red color referred to the liquid region [30]. The white sections denoted the solid-liquid mixed regions [30].

In terms of binary sub-systems, the two thermodynamic databases contained the same binary phases, besides K_4SiO_4, which was added in FToxid based on Kim et al. [28]. FToxid included two ternary phases in the ternary system, $K_2Ca_6Si_4O_{15}$ and $K_2Ca_2Si_2O7$ (called O15 and O7, respectively), which are absent in GTOX. However, the thermodynamic data of these two ternary phases were never measured and were only based on estimations [24]. Other ternary compounds, such as $K_4CaSi_3O_9$, $K_2Ca_3Si_6O_{16}$, and $K_2Ca_2Si_9O_{21}$, were calculated at equilibrium using the GTOX database at 850°C and 1000°C but were not at equilibrium at 1000°C using FToxid. Most importantly, the positions of the various tie lines (equilibrium lines), solidus, and liquidus lines differed between the two databases.

To better understand the differences between the two databases, the standard enthalpy and entropy of formation of the ternary compounds in terms of the pure simple oxides CaO, K_2O and SiO_2-quartz in each database were calculated at 25°C (298K). They are shown in Table 3. This table included values for only the phases found in the calculated ternary phase diagrams CaO-K_2O-SiO_2 at 850°C, 1000°C, and 1200°C. The values in this table highlight the first factor leading to the different ternary diagrams calculated using each database, as shown in Figure 1. From the data in Table 3, although the values of the binary compounds were similar, those of the ternary compounds were different. This difference highly affected the tie line and the equilibria between the compounds. Another factor was the addition of O15 and O7, which changed the whole equilibrium, especially in the central section of the diagram. One last factor may be the different models used to describe the thermodynamic properties of the liquid phase (the associate model in GTOX vs. the quasichemical model in FToxid) applied in each database.

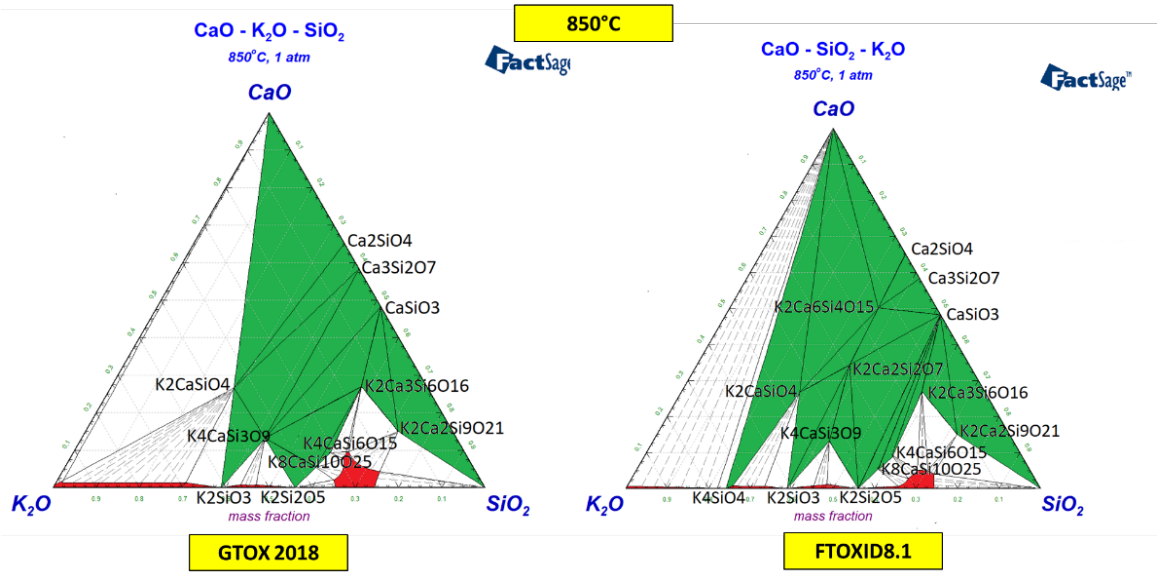

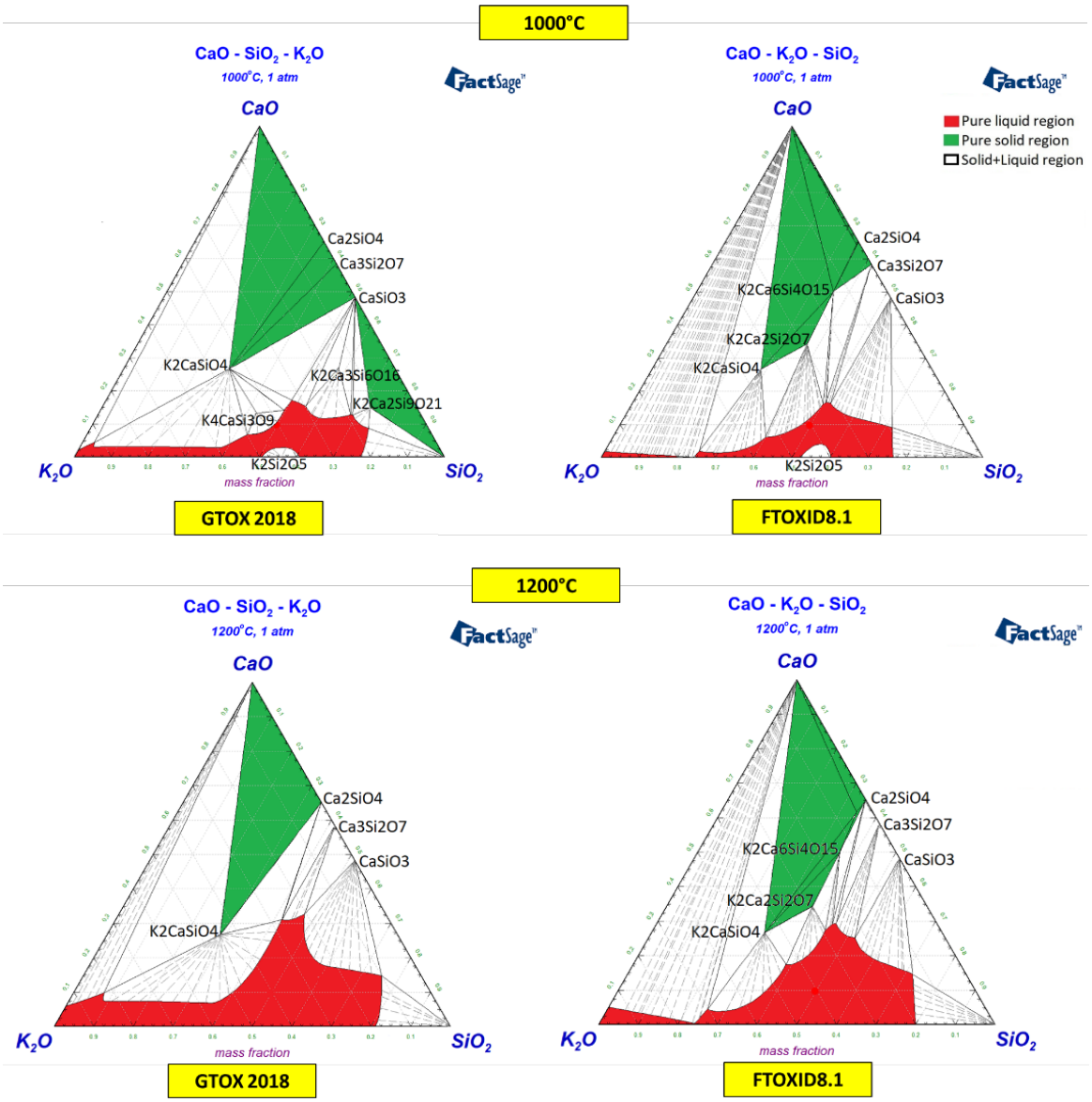

Figure 1: Calculated ternary phase diagrams CaO-K_2O-SiO_2 at 850°C, 1000°C, and 1200°C using GTOX and FToxid.

Table 3: Comparison between GTOX and FTOXID in terms of the enthalpy and entropy of formations at 298K of binary and ternary compounds.

	FTOXID 8.1		GTOX 2018	
	ΔHf (kJ)	S° (J/mol.K)	ΔHf (kJ)	S° (J/mol.K)
K2CaSiO4	-297.71	196.49	-381.68	172.29
K2Ca2Si2O7	-430.92	268.55		
K2Ca6Si4O15	-740.16	490.49		
K4CaSi3O9	-654.81	380.00	-906.83	213.80
K4CaSi6O15	-686.71	564.00	-761.37	515.64
K8CaSi10O25	-1391.92	897.00	-1534.78	800.00
K2Ca2Si9O21	-537.02	558.30	-639.02	500.00
K2Ca3Si6O16	-569.03	512.50	-684.99	428.45
Ca2SiO4	-126.63	119.66	-140.28	120.57

Ca3Si2O7	-223.76	205.56	-225.60	210.89
CaSiO3	-88.89	79.81	-88.43	81.99
K4SiO4	-412.20	245.47		
K2SiO3	-271.60	146.15	-287.96	146.15
K2Si2O5	-320.80	190.58	-339.44	182.00

3.1.2. Global simulation approach

Figure 2 shows the variation of the predicted amounts of the crystalline solids (Figures 2.a and 2.c) and the volatilization behavior (Figure 2.b and 2.d) as a function of the changes of the bark weight fraction in the BC-WC ash mixture at 1000°C. Figures 2.a and 2.b shows the predicted results using the GTOX dataset 1. Figures 2.c and 2.d presented those predicted using the FToxid dataset 2. The previous phase diagram approach used Ca, K, and Si oxides in the prediction (atmosphere absent, so no volatilization prediction), while the global approach used all the elements in the calculations, considering the air atmosphere.

Comparing the predicted solid and liquid phases using the GTOX dataset (Figure 2.a) and the FToxid dataset (Figure 2.c), more liquid phase contents and higher Ca_2SiO_4 and $Ca_3Si_2O_7$ contents were predicted using the GTOX dataset than the FToxid dataset. In addition, the stability range of Ca_2SiO_4 was wider in the calculated results using the GTOX dataset than the those using the FToxid dataset. Most importantly, K_2CaSiO_4 was not at equilibrium in the simulation using FToxid, while $K_2Ca_6Si_4O_{15}$ was absent from the GTOX database. Calculations using the FToxid dataset predicted several minor phases with Mg and Al, while those using the GTOX dataset failed to do that. $CaSiO_3$ and the potassium-based phases such as K_3PO_4, $KAlSiO_4$, and $KAlO_2$ found with FToxid calculations were also absent from those using GTOX. In GTOX, a slag solution phase called LIOS is modeled. This solution dissolves oxides, metals, sulfides, sulfates, and fluorides. Consequently, the K-bearing compounds must have dissolved within this slag phase.

On the other hand, several potential liquid solution descriptions are available in the FToxid 8.1 database called Slag A or Slag B. According to the documentation file of the FToxid database, slag A is a liquid solution of various oxides that can dissolve sulfur as sulfides. Therefore, it is more used in literature than slag B [31–33]. In contrast, the FactSage description of Slag B says that it is a liquid solution of various oxides that can dissolve sulfur as sulfates as a dilute solution with a maximum concentration of 10 wt.%. Sulfates, especially in the form of K_2SO_4, rather than sulfides, are generally found in the biomass ash. Hence, Slag B is usually chosen for feedstock rich in sulfur due to its ability to handle both silicates and sulfates interactions with various positively charged ions [34] and accommodate for SO_3 dissolution [35]. However,

according to the documentation file of the FToxid database, slag B was never optimized for the system CaO-K_2O-SiO_2. Consequently, Slag A was chosen in FToxid in all experimental simulations in this work rather than Slag B.

A detailed analysis of the effect of using Slag A vs. Slag B and adding FTSalt to the experimental simulations is presented in Appendices B and C. From Figure B in Appendix B, adding the FTSalt database to the experimental simulations in dataset 2 did not significantly affect the predicted condensed phases and volatilization. In addition, from the results in Appendix C, using slag B in the simulations rather than slag A destabilized several major K-rich phases found experimentally, such as $KAlSiO_4$, $K_2Ca_6Si_4O_{15}$, and $K_2Ca_2Si_2O_7$. This is because K was dissolved in slag B instead of reacting with alkaline earth-silicate compounds. Hence, simulations using this slag increased the liquid contents and the amounts of some alkaline earth-silicate binary phases, such as $Ca_3Si_2O_7$ and Ca_2SiO_4.

The clear difference between the two databases can be highlighted by taking the 50-50 bark-straw ash mixture (β) case (BCWC) in Figure 2, as an example. Using the GTOX dataset (Figure 2.a), liquid, $Ca_3Si_2O_7$, Ca_2SiO_4, and K_2CaSiO_4 were present in the mixture at equilibrium. On the contrary, using the FToxid dataset (Figure 2.c), less liquid and minor amounts of $Ca_3Si_2O_7$ were present. In addition, the primary crystalline solid was $K_2Ca_6Si_4O_{15}$ in the simulations using FToxid instead of the $Ca_3Si_2O_7$ and K_2CaSiO_4 in those using GTOX. Again, all these differences may be related to the different liquid phase models (the associate model in GTOX vs. the quasichemical model in FToxid) and their extrapolation into the ternary system as well as the different compounds and their thermodynamic data (Table 3) used in each database.

In terms of elemental volatilization, according to Figures 2.b and 2.d, both databases predicted full C and Cl volatilization in the form of CO_2(g), KCl(g), and K_2Cl_2(g). Both databases showed minor differences of K and Na predicted volatilization. Besides, slightly higher Na volatilization was predicted using the GTOX dataset at β higher than 0.7 (bark rich region). The predicted volatilizations for the rest of the inorganic elements were negligible and were omitted from Figures 2.b and 2.d.

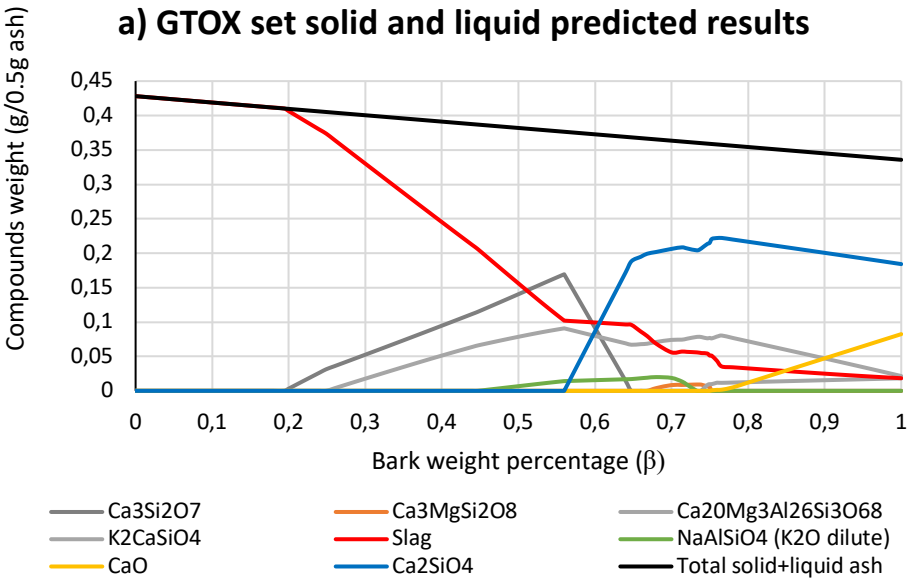
a) GTOX set solid and liquid predicted results
Compounds weight (g/0.5g ash)
0,45
0,4
0,35
0,3
0,25
0,2
0,15
0,1
0,05
0
0
0,1
0,2
0,3
0,4
0,5
0,6
0,7
0,8
0,9
1
Bark weight percentage (β)
Ca3Si2O7
Ca3MgSi2O8
Ca20Mg3Al26Si3O68
K2CaSiO4
Slag
NaAlSiO4 (K2O dilute)
CaO
Ca2SiO4
Total solid+liquid ash

333

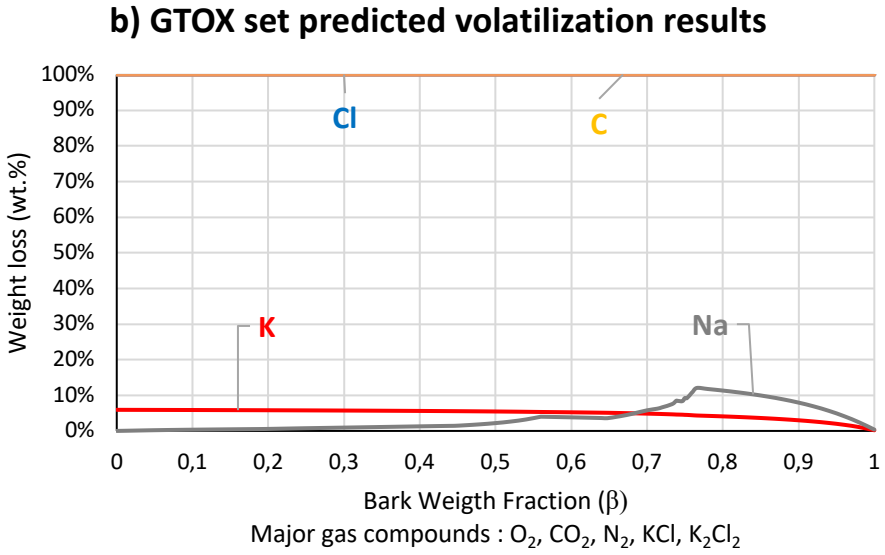
b) GTOX set predicted volatilization results
Weight loss (wt.%)
100%
90%
80%
70%
60%
50%
40%
30%
20%
10%
0%
Cl
C
K
Na
0
0,1
0,2
0,3
0,4
0,5
0,6
0,7
0,8
0,9
1
Bark Weigth Fraction (β)
Major gas compounds : O_2, CO_2, N_2, KCl, K_2Cl_2

334

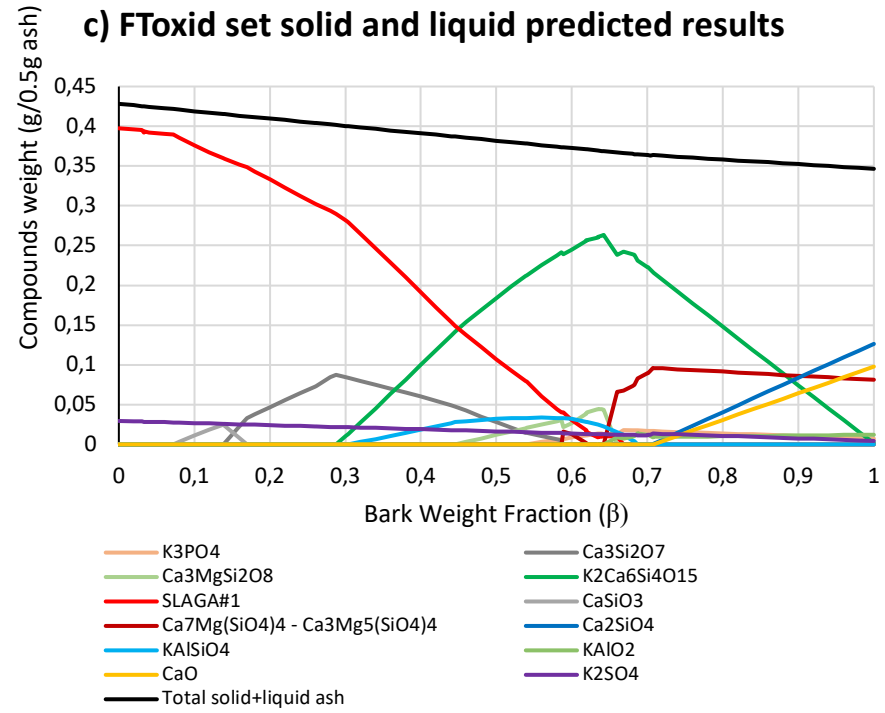

335

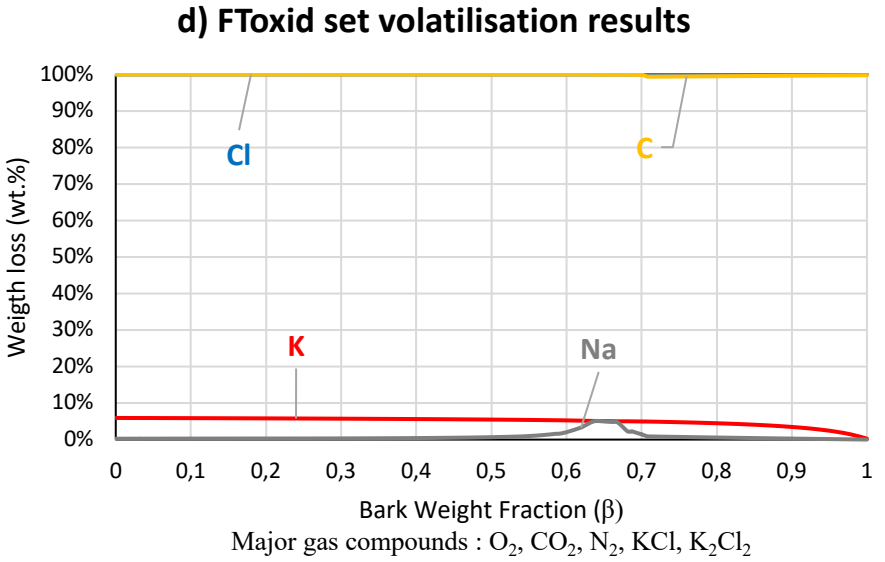

336

337 *Figure 2: Global simulation at various BC weight fraction in WC-BC ash mixture calculated at 1000°C using GTOX (a,b)*
338 *and FToxid (c,d) database sets.*

339 ## 3.2. Comparison between the phase diagram approach and the global simulation
340 approach

341 To compare the prediction capabilities between the phase diagram and the global simulation
342 approaches, calculations were conducted using the same inorganic elements Ca, K, and Si.
343 Hence, the global simulation in this section was done using C, H, N, and O along with Ca, K,
344 and Si elements. The FTOXID dataset 2 (with FactPS and FTSalt) was used at 1000°C (Figure

345 3). The elemental compositions of BC and WC from Table 1 were used as input data. The other
346 barks and straws exhibited similar behavior, along with their mixtures.

347 No inorganic volatilization was found with the global simulation approach. The condensed
348 predicted phases (Figure 3) agreed with the phase diagram calculation (Figure 4). To illustrate
349 this, in Figure 4, the ash of pure bark (BC) started in a three-phase region (CaO-Ca_2SiO_4-
350 $K_2Ca_6Si_4O_{15}$) and then moved into another three-phase region as the bark weight fraction
351 decreased in the mixture until β=0.85 (CaO-$K_2Ca_6Si_4O_{15}$-K_2CaSiO_4). Beyond this
352 composition, as the ash bark contents β further decreased, reaching 0.65, $K_2Ca_2Si_2O_7$
353 appeared and replaced CaO in the three-phase region. Liquid appeared at β=0.6, where the
354 mixture stayed in a $K_2Ca_2Si_2O_7$-$K_2Ca_6Si_4O_{15}$-liquid three-phase region until β=0.28. For
355 $0.05<\beta<0.28$, the mixture was in the $K_2Ca_2Si_2O_7$-liquid two-phase region, after which it
356 reached the pure liquid region for pure straw WC. The pathway mentioned above from the
357 global simulation was precisely according to the proposed phase diagram pathway drawn as
358 the yellow line in Figure 4. In conclusion, the two approaches exhibited the same behavior
359 when the same elements were used. This was mainly due to the absence of K-volatilization in
360 the global simulation approach.

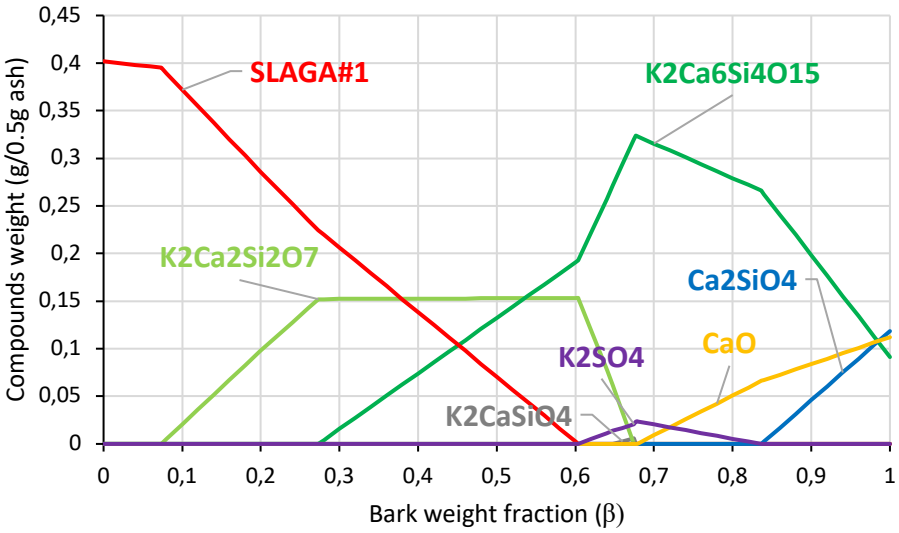

361

362 *Figure 3: Global simulation at 1000°C using FToxid as database and CaO, SiO_2, and K_2O as inorganic oxides between WC*
363 *and BC ashes.*

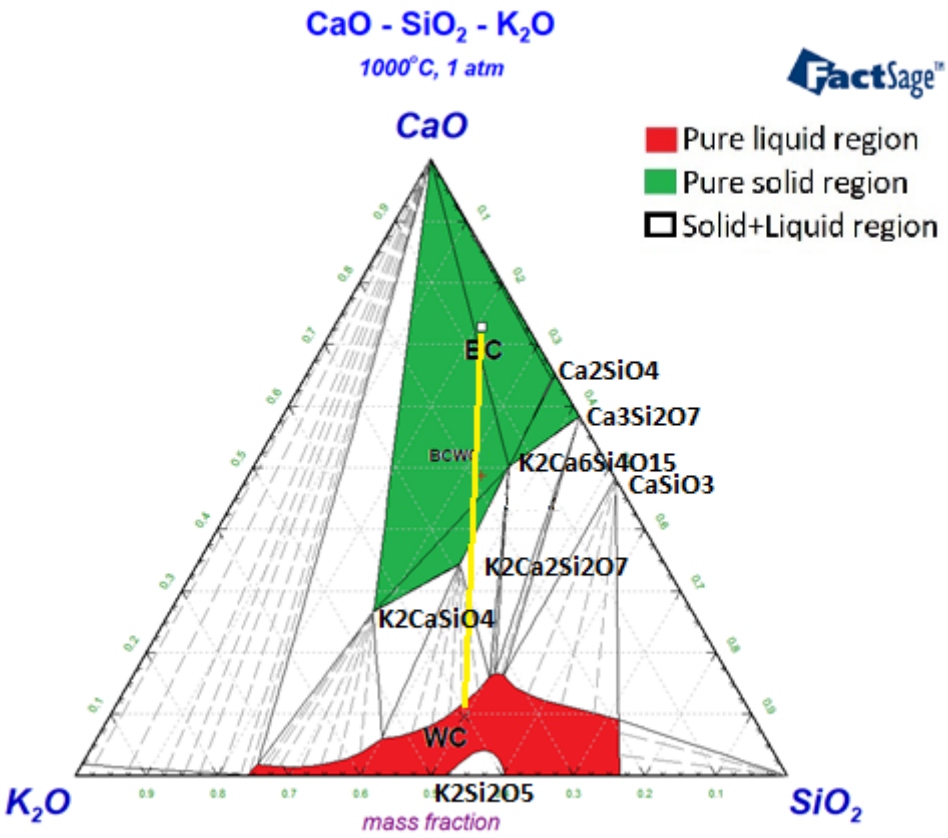

Figure 4: Ternary phase diagram CaO-K_2O-SiO_2 using FToxid 8.1 at 1000°C.

However, some differences were observed when comparing the global simulation results in Figure 2.c (using all elements) against those in Figure 3 (using only 3 oxides). $K_2Ca_2Si_2O_7$ was present among the phases predicted by the simulations in Figure 3 (using only 3 oxides), while it was absent from the predicted results using all elements (Figure 2.c) at the expense of more liquid. In parallel, Ca, Si, and especially K volatilization in the three elements simulation were negligible. In contrast, a moderate K volatilization (as KCl, K_2Cl_2) in the case of the full element global simulation (Figure 2.d) was found in the range of 8 wt.% as β varied. Hence, it was clear that another inorganic element (i.e. S, Cl, Na, Mg, P, Fe, or Mn) was increasing K volatility and destabilizing $K_2Ca_2Si_2O_7$.

To further investigate this effect, simulations were repeated, adding one element X (X denoted Mn, Na, Fe, Al, S, Mg, Cl, and P) to the combination C, H, O, N, Ca, K, and Si. FToxid oxide solution Slag A was always used. The detailed results are shown in Appendix A. From Figure A.1 in Appendix A, the addition of each new element X led to the addition of crystalline solids and solutions linked to it, like $KAlSiO_4$ and $KAlO_2$ in the case of Al (i.e., for the CHNOCaKSiAl system), $Ca_3Fe_2Si_3O_{12}$ in the case of Fe (CHNOCaKSiFe), and more. Nevertheless, this single addition kept $K_2Ca_2Si_2O_7$ stable and K volatility negligible. As a result,

more elements were added to the initial combinations, and simulations were repeated to analyze further the combination of elements that destabilized $K_2Ca_2Si_2O_7$ and increased K volatility.

In conclusion, this phase was found to be stable in the presence of the various combinations of CHNOCaKSi with Al, S, Fe, Mn, and Na (Figure A.2). However, the elements that were found to destabilize $K_2Ca_2Si_2O_7$ were P, Cl, and Mg: P (Figure A.3) due to its competition with K and Ca on the silicate matrix, Cl (Figure A.4) due to its reaction with K to produce KCl(g) in the gaseous phase, and Mg (Figure A.5) by its substitution reaction with Ca. As a result, the simulations validated that several minor inorganic elements can affect the predicted ash behavior.

3.3. Assessing the prediction capabilities with respect to experimental data

In this section, the predicted solid and liquid phases along with volatilization were compared to experimental data obtained at thermodynamic equilibrium [26] using the ash of single biomasses and their ash mixtures presented in Tables 1 and 2. The experimental data were recorded at 1000°C for six biomasses and eight ash mixtures. In addition, three temperatures (850°C, 1000°C, and 1200°C) were studied for the mixture BCWC (called MP2b in the work of Atallah et al. [26] and Defoort et al.[9]).

To assess the prediction capabilities of the phase diagram approach, the single biomasses ashes were positioned in the CaO-K_2O-SiO_2 phase diagram calculated at 1000°C in Figure 5, based on their CaO, SiO_2, and K_2O weight percentages shown in Tables 1 and 2. For simplicity, results only at 1000°C were shown in Figure 5 using each database. Similar outcomes were seen at 850°C and 1200°C.

3.3.1. Single biomass ash case

Figure 6 shows the measured P-XRD results for each straw and bark ash compared to those predicted by the global simulation approach using each database set at 1000°C.

In Figure 5, the three straws were located in the pure liquid region. Accordingly, the P-XRD results in Figure 6 showed that all the measured wheat straw samples at 1000°C were in the liquid phase with minor K_2SO_4 concentration (< 10 wt.%). The amorphous contents was proportional to the alkali-silicate oxide contents and inversely proportional to the one of alkaline earth metal oxide [6,36]. Hence, the measured amorphous contents in the straw ash samples in Figure 6 could be ranked similarly to their K_2O weight percentages (Table 1), in the following increasing order: WF < WI < WC. In terms of predictions, simulations using the GTOX dataset failed to predict the presence of K_2SO_4 in the three straws, showing instead a

total solubility of K and S in the liquid phase LIOS. In contrast, calculations using FToxid set successfully predicted the straw behavior with a minor quantitative difference with the P-XRD measured values (<5% absolute error).

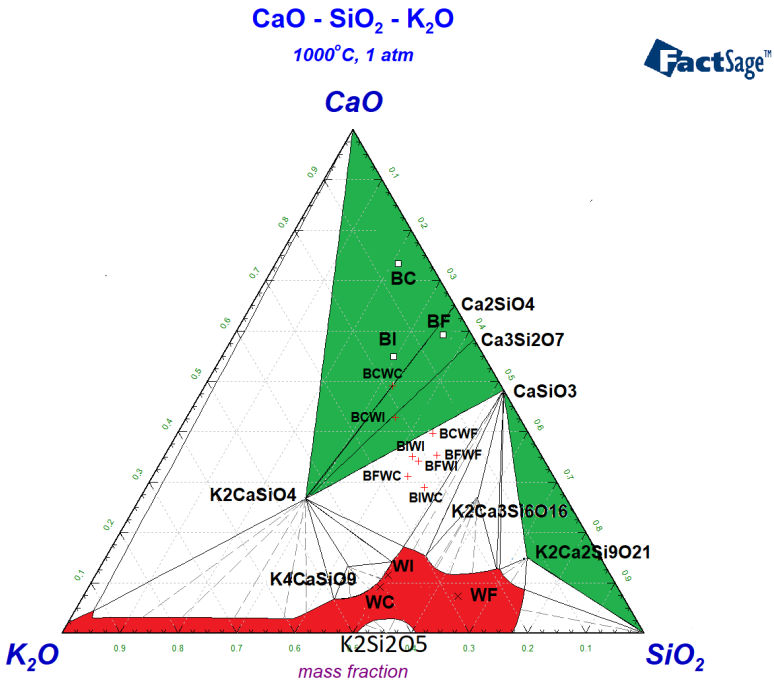

GTOX

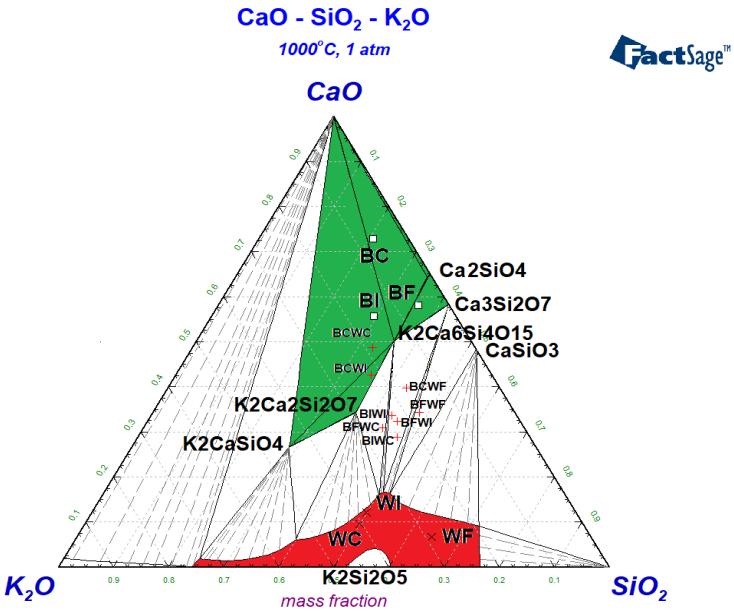

FToxid

Figure 5: Position of the various single biomasses and their mixtures in the form of ash in the phase diagram calculated at 1000°C using GTOX and FToxid

On the other hand, the three barks were located in the pure solid region in Figure 5. Accordingly, from Figure 6, all the measured oak bark samples showed low amorphous contents (<30 wt.%).

It should be noted that the measured amorphous contents contain molten ash mixed with tiny crystals of µm in size. Hence, the effective measured liquid contents had to be less than 30 wt.%. As a result, the phase diagram approach provided a good ash state prediction for single barks cases.

According to Table 1, BF was mostly rich in Si among the three bark samples. Hence, it presented the highest amorphous contents among the three barks. BC and BF presented close weight percentages of CaO, K_2O, and SiO_2 (Table 1). This explains the close concentration of each phase found in their ashes (Figure 6). BI was the richest in Si, K, Na, P, Fe, and Mg and the poorest in Ca. It contained three times the K contents in BC and BF at the expense of less Ca (Table 1). Therefore, the measured $CaO/(CaOH)_2$ concentration in this sample was the lowest at the expense of the abundance of K_2SO_4 and $KAlSiO_4$ concentrations. Ca_2SiO_4 was present in all the measured samples, while the predicted K_2CaSiO_4 was experimentally absent. This is not surprising as Ca_2SiO_4 is the most stable compound in the CaO-SiO_2 binary system.

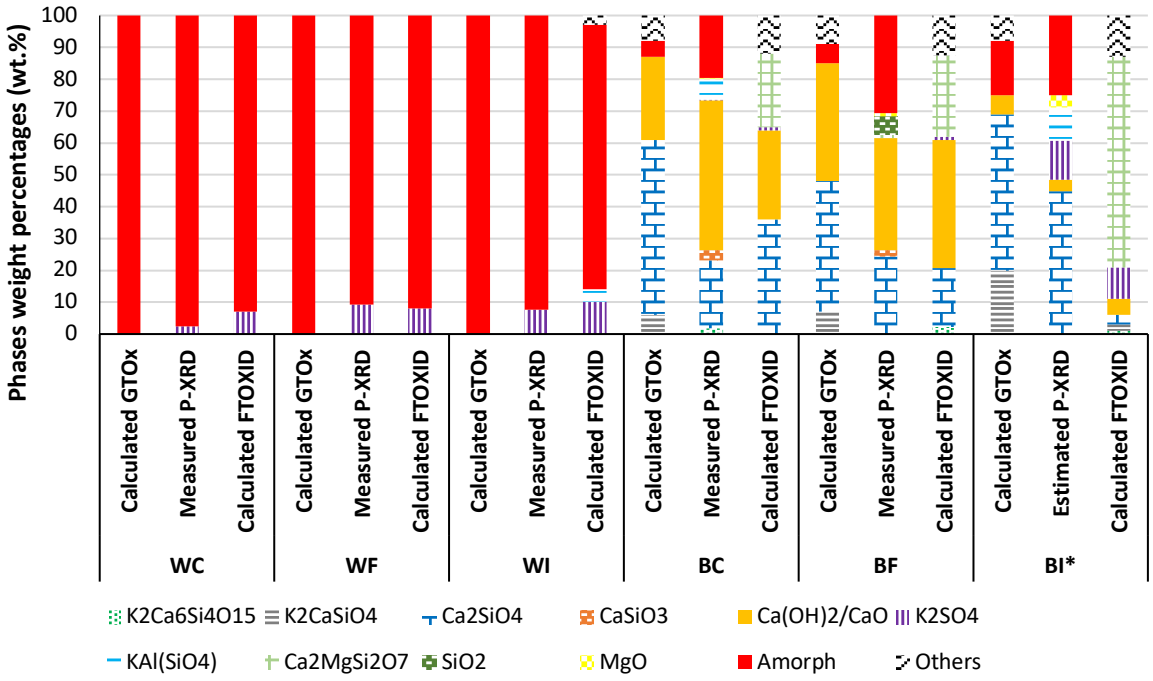

Figure 6: Measured (P-XRD) phases within the ash of the various biomasses versus those predicted by the global simulation using GTOX and FToxid database sets after annealing for 6h at 1000°C. The error for the measured P-XRD results was in the range of 2 wt.%.

**The crystalline/amorphous compositions of BI were estimated based on the amorphous percentage of BC and BF and BI measured XRD compositions without TiO2.*

In terms of predictions, calculations using both databases failed to predict the existence of the minor phases in all bark samples, such as $CaSiO_3$, K_2SO_4, $KAlSiO_4$, SiO_2, and MgO. $Ca_2MgSi_2O_7$, always predicted by the calculations using the FToxid dataset, was never found

experimentally. In contrast, the simulations using the FToxid dataset failed to predict the amorphous contents that were found experimentally, and in the prediction using the GTOX dataset. Nevertheless, an amorphous concentration difference remained between the measured and the predicted values using the GTOX dataset. Both databases showed good prediction capabilities for Ca_2SiO_4 and $CaO/CaCO_3$ crystalline phases. However, the relative quantitative prediction error for these two compounds always ranged between 5% and 50%. Here again, the presence of K_2CaSiO_4 in GTOX always hindered good predictions. In conclusion, despite its success in the case of single straws, the global simulation approach showed some limitations in the case of barks. The ash elemental interactions were more complex in the case of barks than straws, which might have limited the predictions in the case of barks. For instance, the major ash interactions in the case of straws were confined between K and Si, while Ca was present in addition to the first two elements in the case of barks (Table 1).

3.3.2. Biomass ash mixtures

Figure 7 shows the measured P-XRD results for each straw-bark ash mixture compared to those predicted by the global simulation approach using each database set at 1000°C. Figure 8 shows the measured experimental P-XRD results for the BCWC ash mixture at various temperatures compared to those predicted by each database.

According to Figure 5, all mixtures were positioned in the solid-liquid region, besides BCWC and BCWI. The latter was on the border of the solid and solid-liquid region. BCWC was deep in the solid region. Accordingly, from Figure 7, the measured P-XRD concentrations showed crystalline phase mixtures with significant amorphous contents, ranging between 40 wt.% and 60 wt.%. The lowest amorphous contents were seen in the BCWC mixture. As a result, the phase diagram approach using both databases showed good prediction capabilities for the ash state in the case of the blends.

According to Figures 7 and 8, global simulations using the GTOX dataset failed to predict $K_2Ca_6Si_4O_{15}$ and $K_2Ca_2Si_2O_7$, the major ternary phases found experimentally. Unfortunately, they were absent from this database (Table 3). Besides, calculations using the GTOX dataset consistently predicted K_2CaSiO_4 and ranked it as one of the major phases. However, this phase was never found experimentally neither in any mixtures nor in BCWC at various reaction temperatures. This experimental finding was in agreement with the work of Arroyabe et al. [37].

On the other hand, in Figure 7, equilibrium results obtained with the FToxid dataset presented good prediction capabilities for the major ternary phases in the mixtures located in the solid section (green section in Figure 1) or close to it, as BCWC, BFWC, and BCWI. However, the usage of the FToxid dataset failed to offer good predictions in the other mixtures, especially those in the solid-liquid sections (i.e., in the middle section of the diagram). Similarly, in Figure 8, calculation results obtained with FToxid provided better predictions for the measured major phases, especially at 1000°C (equilibrium temperature for $K_2Ca_6Si_4O_{15}$ and $K_2Ca_2Si_2O_7$ [26]), than those using the GTOX dataset.

Simulations using the two databases predicted the presence of the liquid phase coherently with the measurements. However, discrepancies remained between the measured concentrations and those predicted using both databases in the different mixtures (Figure 7) and at different temperatures (Figure 8).

It should be noted that from the results in Figure 7, simulations using the GTOX dataset were able to better predict the presence of Ca_2SiO_4 than using the FToxid dataset for the mixtures in the solid section (green section in Figure 5) or close to it (BCWC, BFWC, and BCWI). However, further improvements are still needed for a better quantitative prediction. For the case of BCWC at different temperatures, the use of both databases failed to predict the presence of Ca_2SiO_4 at 850°C but provided good qualitative and quantitative predictions at 1200°C. Nevertheless, only using the GTOX dataset predicted this phase at 1000°C. The different thermodynamic data applied in each database for this crystalline phase (Table 3) could be the main reason behind this behavior.

$Ca_3Si_2O_7$ was predicted using the two databases but was rarely found experimentally in the various mixtures (Figure 7) and at different temperatures (Figure 8). Its absence could be due to its slow kinetic formation [38]. However, its predicted appearance in the mixtures was always conjugated with the experimental $CaSiO_3$ appearance (Figure 7). The latter was never predicted by any database.

In terms of minor compounds, simulations using the GTOX dataset could not predict the K-rich compounds (with aluminum and sulfur) found experimentally, according to Figures 7 and 8, such as $KAlSiO_4$ and K_2SO_4. Instead, they were predicted to dissolve in the LIOS slag solution in the GTOX database modeling. Though simulations using the FToxid dataset were able to predict the presence of these experimental phases, it needed further improvement in terms of predicted concentrations. Furthermore, the only minor compound, $NaAlSiO_4$, predicted in

certain mixtures using GTOX calculations, was never found experimentally. Hence, using the GTOX dataset for the simulations showed clear limitations for predicting the minor phases. Calculations using the FToxid dataset behaved better but still needed further improvements.

The disagreement between the measured and predicted major crystalline phases along with the liquid contents can be due to the estimated thermodynamic data of $K_2Ca_6Si_4O_{15}$ and $K_2Ca_2Si_2O_7$ in FToxid. It can also result from the thermodynamic extrapolation of the liquid phase from the binaries. Once the missing / estimated properties are measured and added to the database, and if this system is remodeled after excluding K_2CaSiO_4, the tie lines and phase equilibria may change. This update can induce significant modifications to the predicted results, especially for the samples in the central section of the ternary diagram. This remodeling may also increase the quantitative prediction capabilities of the thermodynamic approach/database. In conclusion, simulations using the FToxid database showed clear advantages over those using GTOX, but both databases need further improvements.

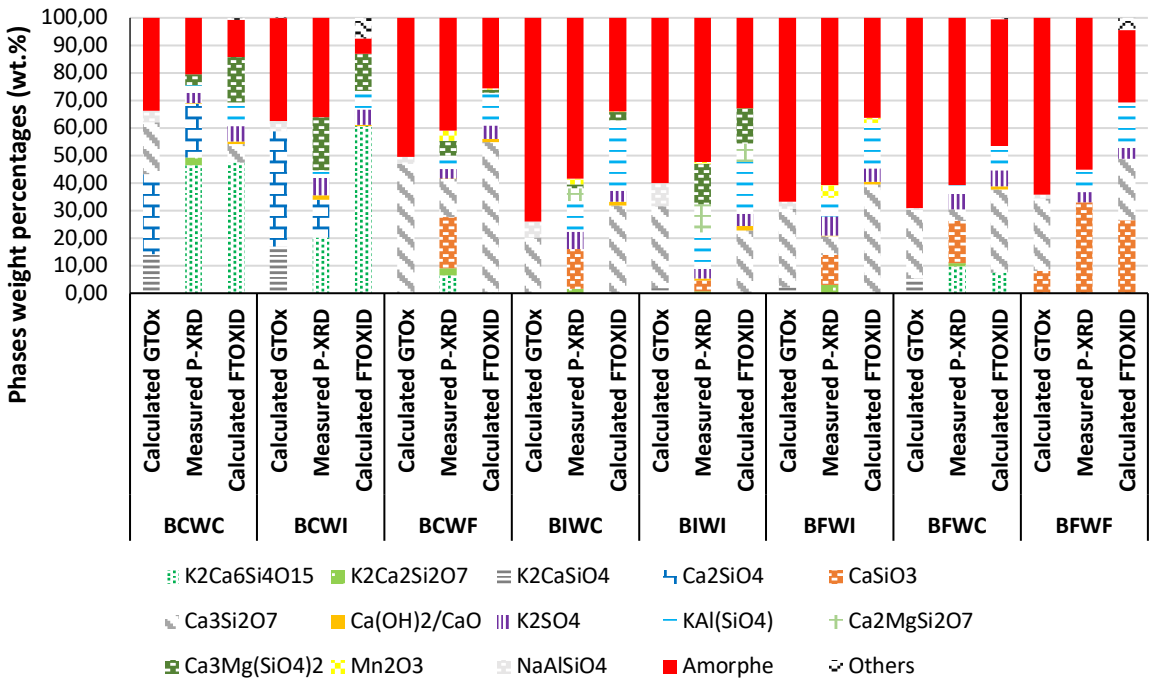

Figure 7: Measured (P-XRD) phases within the ash of the various mixtures vs. those predicted by the global simulation using GTOX and FToxid database sets after annealing for 6h at 1000°C. The error for the measured P-XRD results was in the range of 2 wt.%.

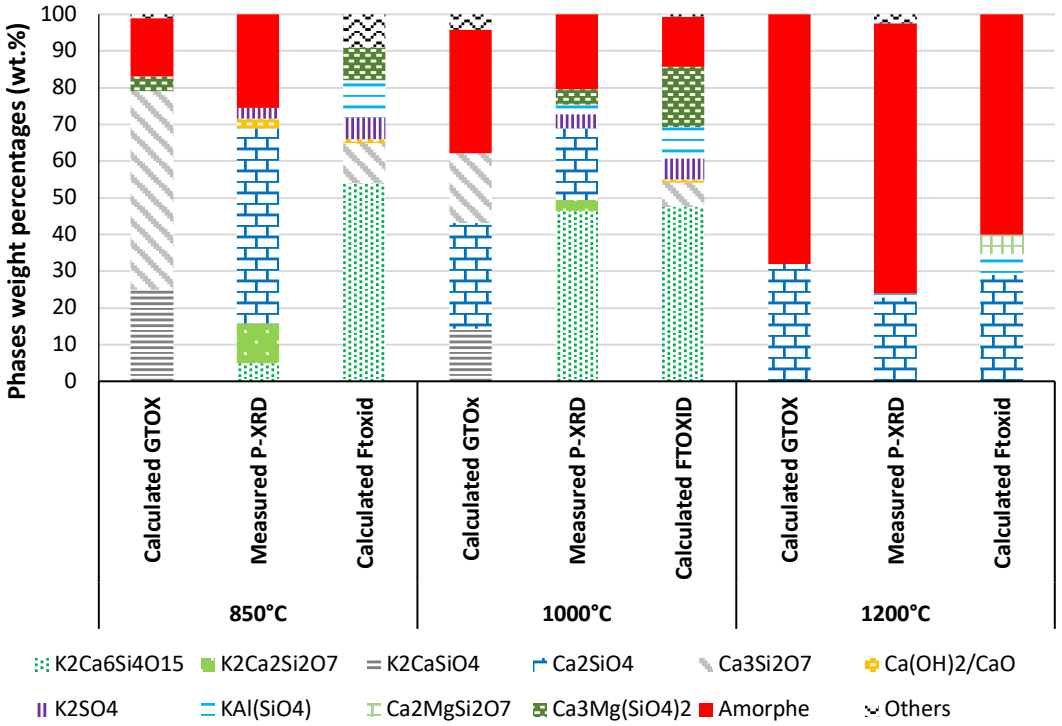

Figure 8: Predicted phases by the global simulation approach using GTOX and FToxid database sets vs. those measured (P-XRD) within the ash of the BCWC mixture after annealing for 24h at 850°C, 6h at 1000°C, and 6h at 1200°C. The error for the measured P-XRD results was in the range of 2 wt.%.

3.3.3. Total and elemental volatilization

To further assess the capabilities of the thermodynamic tool to predict the annealing experiments of ash, total and elemental volatilization (K, Na, and C) predicted by FToxid and GTOX were compared to those measured experimentally in Figure 9 for the BCWC ash mixture. It should be noted that the volatilization for the rest of the inorganic elements was negligible (both in the measurements and the predictions).

As shown in Figure 9.a, the predicted total volatilization values from the two databases were analogous. In addition, they were close to the dynamic total volatilization measured by the TGA-DTA, especially at temperatures higher than 850°C. This temperature is considered the minimum operating temperature of any combustion process in general [39,40]. However, the total volatilization at temperatures lower than 850°C was different between the predicted and the dynamically measured results. For instance, carbon volatilization was predicted to increase below 850°C gradually. However, this volatilization happens faster in real-life processes. In addition, the predicted total volatilization was also consistent with the three static total volatilizations measured with the ash test (i.e., total experimental weight loss between the beginning and the end of the experimental test).

In parallel, the percentage of error of the method used to calculate the elemental volatilization from the measured ICP-AES values reached 15%. Hence, from Figure 9.b, it can also be concluded that simulations using both databases were able to predict potassium, sodium, and carbon volatilization efficiently. The total volatilization of carbon and the significant loss of K, S, and Na into the gaseous phase, which were found experimentally, also agreed with the literature. Bostrom et al. [36] ranked the stability of oxides in the following increasing order: $K_2O<Na_2O<SO_2<H_2O/P_2O_5<CO_2<CO<SiO_2<MgO<CaO$. Hence, at a high availability of oxygen, such as in the combustion mode, carbon will be totally lost into the gaseous phase in the form of CO_2(g) and CO(g) [41]. Alkali oxides (K_2O and Na_2O) will primarily react with water vapor and volatilize fast in the form of KOH(g) and NaOH(g) [10,36]. Sulfur has a lower affinity to oxygen than to carbon and hydrogen [36]. Hence it will initially be released in the form of H_2S to further oxidize in excess oxygen to form SO_2 and later SO_3 in the gaseous phase [36,41]. Similarly, chlorine, which is considered an unstable oxide, will easily volatilize in the form of KCl(g), Cl_2(g), and HCl(g) vapor due to their low stability bonds with oxygen [42].

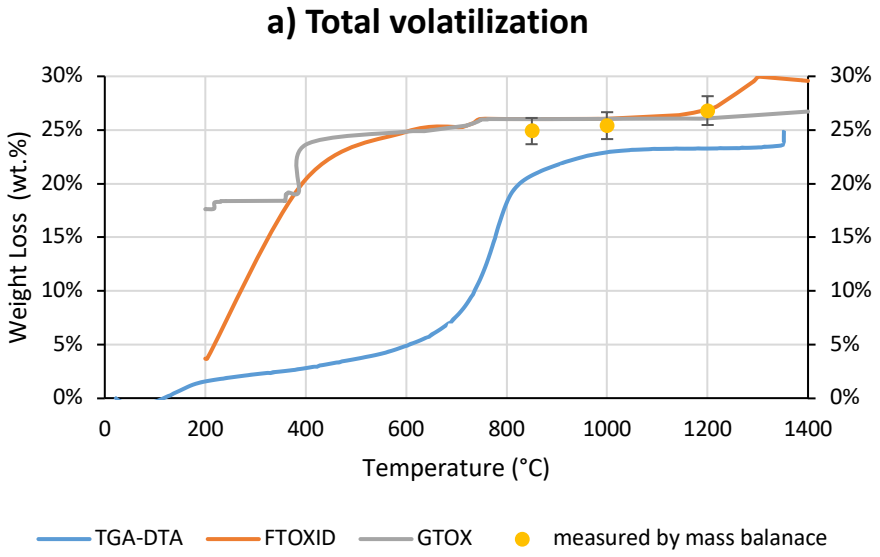

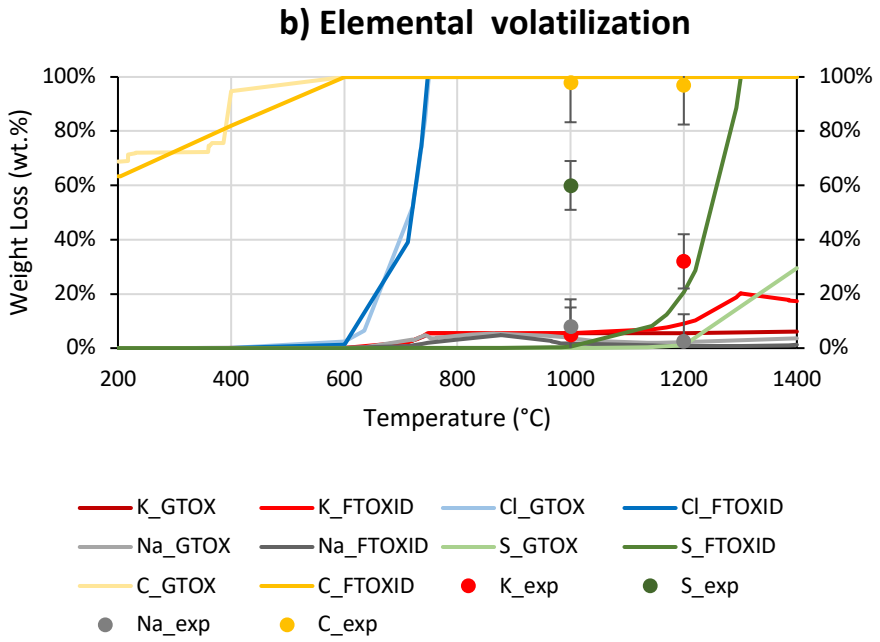

Figure 9: Predicted and measured total (a) and elemental (b) volatilization for the BCWC ash mixture.

3.3.4. Characteristic temperatures

Table 4 shows the solidus and liquidus temperatures for the BCWC mixture as measured by TGA-DTA (Appendix D) and compared with those predicted. Calculations using the FToxid and GTOX databases predicted a close liquidus temperature of around 1400°C while showing a 100°C difference in the solidus temperature. Though the liquidus temperature of the mixture was not able to be measured due to experimental limitations, the experimental solidus temperature was 1180°C, significantly higher than those predicted. This finding again highlighted the limitation of the current thermodynamic databases and the need for corrections. The work of Berjonneau et al. [43] confirmed the findings in this work. In one of the rare literature references that tried to compare the measured and predicted liquidus temperatures in the biomass ash, these authors annealed and then analyzed synthesized ash samples with close compositions to straw and miscanthus ashes, with and without K_2O contents [43]. They conducted their prediction using the same approach in this work. Berjonneau et al. [43] found close measured and predicted liquidus temperatures for miscanthus ash samples synthesized without K_2O. However, when K_2O was added to the ash sample, the measured liquidus temperatures drastically decreased, and the deviations between the measured and the predicted values increased [43]. Similar to the current work, Berjonneau et al. [43] said that the lack of measured thermodynamic data for the K-compounds in the database highly affected the calculated liquidus temperatures.

582 *Table 4: Solidus and liquidus measured by TGA-DTA and predicted by each database for the BCWC ash mixture.*

	Solidus	Liquidus
TGA-DTA	1180°C	Undetected up until 1350°C
FTOXID prediction	878°C	1400°C
GTOx prediction	748°C	1436°C

583 # 4. Conclusion

584 A critical assessment was carried out of two thermodynamic-based approaches to predict the
585 interactions between the inorganic elements in the ash of biomass and their mixtures. Rather
586 than picking one thermodynamic database package, a comparison between the calculated results
587 using two typical commercial databases (FToxid vs. GTOX) was conducted for the first time.
588 In addition, as part of ongoing work to provide an accurate thermodynamic database, the
589 simulated results using the most recent versions of two thermodynamic database sets were
590 compared against experimental values, highlighting the need for improvements. Several
591 conclusions can be drawn out from this assessment:

592 - Critical differences could be seen between the results predicted by each database in the
593 phase diagram and the global simulation approaches. This was due to the adoption of
594 different solid compounds between the databases, especially after adding $K_2Ca_2Si_2O_7$
595 and $K_2Ca_6Si_4O_{15}$ in FToxid that were absent in GTOX. Considerable differences in the
596 modeled thermodynamic properties of the common ternary compounds were also
597 present. In addition, different liquid models were also used in both databases, which has
598 an impact on the extrapolation of the binary liquid into the ternary system.
599 - The phase diagram and the global simulation approach predicted similar results when
600 the inputs were the same. However, the second approach performed better since it
601 accounted for the volatilization and the interactions between the minor elements.
602 - The phase diagram approach showed excellent capabilities in predicting the ash (solid
603 or liquid) state using both databases.
604 - Using the global simulation approach, simulations using the FToxid dataset offered
605 good qualitative and quantitative predictions for the single biomass ash. It also showed
606 decent qualitative prediction capabilities for the ash mixtures far from the central section
607 of the ternary diagram.
608 - The global simulation prediction failed using both database sets in the case of the
609 mixtures located in the central section of the ternary diagram.
610 - Both databases showed excellent volatilization prediction capabilities. Nevertheless,
611 they failed to forecast the characteristic temperatures for phase transitions.

Further corrections and improvements are still needed, especially in the central section of the diagram. Measuring the estimated thermodynamic properties of $K_2Ca_2Si_2O_7$ and $K_2Ca_6Si_4O_{15}$, and removing the K_2CaSiO_4 compound from this system can significantly enhance the prediction capabilities. Afterward, the improved database can be used to reassess the capabilities of the two thermodynamic approaches to predict the ash behavior in biomass and their mixtures, not only in combustion mode but in gasification too. In addition, the improved database must be tested on mixtures of biomass where reactivity/interactions are lower than in the mixtures of ash of biomass that were used in this work.

Acknowledgment

This work has been supported by the French Commission for Atomic and Alternative Energies (CEA) and the French Institute "Carnot Energies du future"

References

[1] G.W. Morey, F.C. Kracek, N.L. Bowen, The ternary system K2O-CaO-SiO2, J. Soc. Glass Technol. 14 (1930) 149–187.

[2] B. Mysen, P. Richet, Silicate Glasses and Melts, Elsevier, 2019. https://doi.org/10.1016/C2018-0-00864-6.

[3] H. Tripathi, S. Kumar Hira, A. Sampath Kumar, U. Gupta, P. Pratim Manna, S.P. Singh, Structural characterization and in vitro bioactivity assessment of SiO2–CaO–P2O5–K2O–Al2O3 glass as bioactive ceramic material, Ceram. Int. 41 (2015) 11756–11769. https://doi.org/10.1016/j.ceramint.2015.05.143.

[4] S.V. Vassilev, D. Baxter, L.K. Andersen, C.G. Vassileva, An overview of the chemical composition of biomass, Fuel. 89 (2010) 913–933. https://doi.org/10.1016/j.fuel.2009.10.022.

[5] P. Thy, B.M. Jenkins, R.B. Williams, C.E. Lesher, R.R. Bakker, Bed agglomeration in fluidized combustor fueled by wood and rice straw blends, Fuel Process. Technol. 91 (2010) 1464–1485. https://doi.org/10.1016/j.fuproc.2010.05.024.

[6] A. Rebbling, P. Sundberg, J. Fagerström, M. Carlborg, C. Tullin, D. Boström, M. Öhman, C. Boman, N. Skoglund, Demonstrating Fuel Design To Reduce Particulate Emissions and Control Slagging in Industrial-Scale Grate Combustion of Woody Biomass, Energy Fuels. 34 (2020) 2574–2583. https://doi.org/10.1021/acs.energyfuels.9b03935.

[7] M. Öhman, A. Nordin, B.-J. Skrifvars, R. Backman, M. Hupa, Bed Agglomeration Characteristics during Fluidized Bed Combustion of Biomass Fuels, Energy Fuels. 14 (2000) 169–178. https://doi.org/10.1021/ef990107b.

[8] V. Andersson, A.H. Soleimanisalim, X. Kong, F. Hildor, H. Leion, T. Mattisson, J.B.C. Pettersson, Alkali-wall interactions in a laboratory-scale reactor for chemical looping combustion studies, Fuel Process. Technol. 217 (2021) 106828. https://doi.org/10.1016/j.fuproc.2021.106828.

[9] F. Defoort, M. Campargue, G. Ratel, H. Miller, C. Dupont, Physicochemical Approach To Blend Biomass, Energy Fuels. 33 (2019) 5820–5828. https://doi.org/10.1021/acs.energyfuels.8b04169.

[10] P. Thy, B.M. Jenkins, C.E. Lesher, S. Grundvig, Compositional constraints on slag formation and potassium volatilization from rice straw blended wood fuel, Fuel Process. Technol. 87 (2006) 383–408. https://doi.org/10.1016/j.fuproc.2005.08.015.
[11] T. Zeng, A. Pollex, N. Weller, V. Lenz, M. Nelles, Blended biomass pellets as fuel for small scale combustion appliances: Effect of blending on slag formation in the bottom ash and pre-evaluation options, Fuel. 212 (2018) 108–116. https://doi.org/10.1016/j.fuel.2017.10.036.
[12] D. Lindberg, R. Backman, P. Chartrand, M. Hupa, Towards a comprehensive thermodynamic database for ash-forming elements in biomass and waste combustion — Current situation and future developments, Fuel Process. Technol. 105 (2013) 129–141. https://doi.org/10.1016/j.fuproc.2011.08.008.
[13] I.-H. Jung, M.-A. Van Ende, Computational Thermodynamic Calculations: FactSage from CALPHAD Thermodynamic Database to Virtual Process Simulation, Metall. Mater. Trans. B. 51 (2020) 1851–1874. https://doi.org/10.1007/s11663-020-01908-7.
[14] K. Hack, T. Dr.Jantzen, M. Müller, E. Yazhenskikh, G. Wu, A novel thermodynamic database for slag systems and refractory materials, 2012.
[15] H. Wiinikka, R. Gebart, C. Boman, D. Boström, M. Öhman, Influence of fuel ash composition on high temperature aerosol formation in fixed bed combustion of woody biomass pellets, Fuel. 86 (2007) 181–193. https://doi.org/10.1016/j.fuel.2006.07.001.
[16] A.-L. Elled, L.-E. Åmand, B.-M. Steenari, Composition of agglomerates in fluidized bed reactors for thermochemical conversion of biomass and waste fuels: Experimental data in comparison with predictions by a thermodynamic equilibrium model, Fuel. 111 (2013) 696–708. https://doi.org/10.1016/j.fuel.2013.03.018.
[17] T. Rizvi, P. Xing, M. Pourkashanian, L.I. Darvell, J.M. Jones, W. Nimmo, Prediction of biomass ash fusion behaviour by the use of detailed characterisation methods coupled with thermodynamic analysis, Fuel. 141 (2015) 275–284. https://doi.org/10.1016/j.fuel.2014.10.021.
[18] M. Reinmöller, M. Klinger, M. Schreiner, H. Gutte, Relationship between ash fusion temperatures of ashes from hard coal, brown coal, and biomass and mineral phases under different atmospheres: A combined FactSage^{TM} computational and network theoretical approach, Fuel. 151 (2015) 118–123. https://doi.org/10.1016/j.fuel.2015.01.036.
[19] A. Magdziarz, M. Gajek, D. Nowak-Woźny, M. Wilk, Mineral phase transformation of biomass ashes – Experimental and thermochemical calculations, Renew. Energy. 128 (2018) 446–459. https://doi.org/10.1016/j.renene.2017.05.057.
[20] H. Beidaghy Dizaji, T. Zeng, H. Hölzig, J. Bauer, G. Klöß, D. Enke, Ash transformation mechanism during combustion of rice husk and rice straw, Fuel. 307 (2022) 121768. https://doi.org/10.1016/j.fuel.2021.121768.
[21] S. Link, P. Yrjas, D. Lindberg, A. Trikkel, V. Mikli, Ash melting behaviour of reed and woody fuels blends, Fuel. 314 (2022) 123051. https://doi.org/10.1016/j.fuel.2021.123051.
[22] S. Fakourian, Z. McAllister, A. Fry, Y. Wang, X. Li, J.O.L. Wendt, J. Dai, Modeling ash deposit growth rates for a wide range of solid fuels in a 100 kW combustor, Fuel Process. Technol. 217 (2021) 106777. https://doi.org/10.1016/j.fuproc.2021.106777.
[23] Y. Zhu, H. Tan, Y. Niu, X. Wang, Experimental study on ash fusion characteristics and slagging potential using simulated biomass ashes, J. Energy Inst. 92 (2019) 1889–1896. https://doi.org/10.1016/j.joei.2018.11.005.
[24] D. Kim, Coupled Experimental Study and Thermodynamic Optimization of the K2O-Na2O-CaO-MgO-Al2O3-SiO2 System, McGill University, Montreal, Quebec, Canada, 2017.

[25] F. Defoort, B. Grangier, T. Chataing, S. Ravel, G. Ratel, S. Valin, Entrained Flow Gasification of Hardwood Bark: Experimental Characterization of Inorganic Matter versus Equilibrium and Viscosity Predictions, Energy Fuels. 35 (2021) 12151–12164. https://doi.org/10.1021/acs.energyfuels.1c00993.
[26] E. Atallah, F. Defoort, M. Campargue, A. Pisch, C. Dupont, Will mixing rule or chemical reactions dominate the ash behavior of biomass mixtures in combustion processes on laboratory and pilot scales?, Fuel. 308 (2022) 122050. https://doi.org/10.1016/j.fuel.2021.122050.
[27] S. Valin, S. Ravel, P. Pons de Vincent, S. Thiery, H. Miller, F. Defoort, M. Grateau, Fluidised Bed Gasification of Diverse Biomass Feedstocks and Blends—An Overall Performance Study, Energies. 13 (2020) 3706. https://doi.org/10.3390/en13143706.
[28] D.-G. Kim, M.-A. Van Ende, P. Hudon, I.-H. Jung, Coupled experimental study and thermodynamic optimization of the K2O-SiO2 system, J. Non-Cryst. Solids. 471 (2017) 51–64. https://doi.org/10.1016/j.jnoncrysol.2017.04.029.
[29] A. Hedayati, H. Sefidari, C. Boman, N. Skoglund, N. Kienzl, M. Öhman, Ash transformation during single-pellet gasification of agricultural biomass with focus on potassium and phosphorus, Fuel Process. Technol. 217 (2021) 106805. https://doi.org/10.1016/j.fuproc.2021.106805.
[30] L. Fusco, F. Defoort, A thermochemical approach based on phase diagrams to characterize biomass ash and select the optimal thermal conversion technology, Undefined. (2016). https://www.semanticscholar.org/paper/A-thermochemical-approach-based-on-phase-diagrams-Fusco-Defoort/9615ef2beea530c59fb277c82b0bb7ce94b3dabc (accessed March 2, 2022).
[31] H. Xiao, Y. Wang, J. Li, Z. Bao, L. Mu, G. Yu, Prediction of coal ash fusibility based on metal ionic potential concentration, J. Energy Inst. 98 (2021) 29–34. https://doi.org/10.1016/j.joei.2021.04.018.
[32] J. Gao, C. Dong, Y. Zhao, X. Hu, W. Qin, X. Wang, J. Zhang, J. Xue, X. Zhang, Vitrification of municipal solid waste incineration fly ash with B2O3 as a fluxing agent, Waste Manag. 102 (2020) 932–938. https://doi.org/10.1016/j.wasman.2019.12.012.
[33] J. Liao, B. Zhao, Phase equilibria study in the system “Fe2O3”-ZnO-Al2O3-(PbO+CaO+SiO2) in air, Calphad. 74 (2021) 102282. https://doi.org/10.1016/j.calphad.2021.102282.
[34] N. Skoglund, L. Bäfver, J. Fahlström, E. Holmén, C. Renström, Fuel design in co-combustion of demolition wood chips and municipal sewage sludge, Fuel Process. Technol. 141 (2016) 196–201. https://doi.org/10.1016/j.fuproc.2015.08.037.
[35] P.Y. Hsieh, Sintering and collapse of synthetic coal ash and slag cones as observed through constant heating rate optical dilatometry, Fuel. 235 (2019) 567–576. https://doi.org/10.1016/j.fuel.2018.08.055.
[36] D. Boström, N. Skoglund, A. Grimm, C. Boman, M. Öhman, M. Broström, R. Backman, Ash Transformation Chemistry during Combustion of Biomass, Energy Fuels. 26 (2012) 85–93. https://doi.org/10.1021/ef201205b.
[37] E. Arroyabe, R. Tessadri, D.M. Többens, V. Kahlenberg, Does K2CaSiO4 Exist? A Phase-Analytical Study in the System K2O-CaO-SiO2 with Implications for the Characterization of Residual Materials: Does K2CaSiO4 Exist?, J. Am. Ceram. Soc. 94 (2011) 2652–2655. https://doi.org/10.1111/j.1551-2916.2011.04397.x.
[38] A. ŠMIGELSKYTĖ, SYNTHESIS, PROPERTIES, AND APPLICATION OF RANKINITE IN THE PRODUCTION OF CO2 CURED CONCRETE, KAUNAS UNIVERSITY OF TECHNOLOGY, 2019. ISBN 978-609-02-1650-7.
[39] J. Zhang, X. Zhang, 15 - The thermochemical conversion of biomass into biofuels, in: D. Verma, E. Fortunati, S. Jain, X. Zhang (Eds.), Biomass Biopolym.-Based Mater.

752 Bioenergy, Woodhead Publishing, 2019: pp. 327–368. https://doi.org/10.1016/B978-0-
753 08-102426-3.00015-1.
754 [40] Z. Luo, J. Zhou, Thermal Conversion of Biomass, in: W.-Y. Chen, J. Seiner, T. Suzuki,
755 M. Lackner (Eds.), Handb. Clim. Change Mitig., Springer US, New York, NY, 2012: pp.
756 1001–1042. https://doi.org/10.1007/978-1-4419-7991-9_27.
757 [41] S.V. Vassilev, D. Baxter, C.G. Vassileva, An overview of the behaviour of biomass
758 during combustion: Part I. Phase-mineral transformations of organic and inorganic
759 matter, Fuel. 112 (2013) 391–449. https://doi.org/10.1016/j.fuel.2013.05.043.
760 [42] J. Royo, P. Canalís, D. Quintana, Chemical study of fly ash deposition in combustion of
761 pelletized residual agricultural biomass, Fuel. 268 (2020) 117228.
762 https://doi.org/10.1016/j.fuel.2020.117228.
763 [43] J. Berjonneau, L. Colombel, J. Poirier, M. Pichavant, F. Defoort, J.-M. Seiler,
764 Determination of the Liquidus Temperatures of Ashes from the Biomass Gazification for
765 Fuel Production by Thermodynamical and Experimental Approaches, Energy Fuels. 23
766 (2009) 6231–6241. https://doi.org/10.1021/ef900738c.
767